

Article

The Power Setting of Focused Ultrasound for the Palliative Treatment of Advanced Pancreatic Cancer: A Study in an Ex Vivo Bovine Liver

Shiqi Tong, Yuebing Wang *, Peng Zhao, Jie Tao, Xiaohan Guo and Yaping Yu

College of Metrology and Measurement Engineering, China Jiliang University, Hangzhou 310018, China

* Correspondence: wyb_1963@163.com; Tel.: +86-(57)-186914558

Abstract: High-intensity focused ultrasound (HIFU) ablation has been widely used in advanced pancreatic cancer in recent years. In numerous studies, HIFU has been shown to be safe, effective, and practicable, but there are a few HIFU-related adverse effects. The patients' discomfort during therapy increased proportionally with increasing delivered energy and pain levels seemed to be independent of the dose of anesthetic or sedation. If the power used in therapy is too high, the temperature of the target area will rise rapidly, and the boiling and cavitation make the shape of the necrosis area difficult to control. In recent years, moderate-intensity focused ultrasound (MIFU) has also been shown to heat the tumor locally for palliative treatment. Choosing the appropriate power and effectively controlling the tissue temperature until reaching the threshold for thermal necrosis are of great significance for ensuring the safety of palliative treatment. In this study, an infrared temperature measurement experimental system was set up to measure the temperature rise at different power in an ex vivo bovine liver. It was found that when the acoustic intensity of the focused ultrasound was lower than the cavitation threshold (within the range of the MIFU), the temperature of the tissue kept rising at a steady rate and could still reach the thermal damage threshold temperature within tens of seconds. The results showed that the temperature induced by the MIFU was almost entirely dependent on the thermal effect, and the temperature of the tissue at the end of sonication was linearly related to the power. Finally, this study considered the effect of blood perfusion on the temperature for the application of focused ultrasound in the palliative treatment of advanced pancreatic cancer with the goal of providing a reference for the application of focused ultrasound in the palliative treatment of advanced pancreatic cancer.

Keywords: pancreatic cancer; palliative treatment; moderate-intensity focused ultrasound; temperature



Citation: Tong, S.; Wang, Y.; Zhao, P.; Tao, J.; Guo, X.; Yu, Y. The Power Setting of Focused Ultrasound for the Palliative Treatment of Advanced Pancreatic Cancer: A Study in an Ex Vivo Bovine Liver. *Appl. Sci.* **2023**, *13*, 474. <https://doi.org/10.3390/app13010474>

Academic Editor: Piero Tortoli

Received: 15 November 2022

Revised: 16 December 2022

Accepted: 27 December 2022

Published: 29 December 2022



Copyright: © 2022 by the authors. Licensee MDPI, Basel, Switzerland. This article is an open access article distributed under the terms and conditions of the Creative Commons Attribution (CC BY) license (<https://creativecommons.org/licenses/by/4.0/>).

1. Introduction

Pancreatic ductal adenocarcinoma (PDA), also known as pancreatic cancer, is projected to become the second leading cause of cancer-related mortality by 2030 [1]. Despite modest advances in conventional systemic therapies, the 5-year overall survival (OS) for PDAC remains a dismal 11% [2], in part because of its advanced stage at presentation precluding curative-intent resection and a high propensity for recurrence [3]. Early-stage pancreatic cancer usually has no symptoms. When symptoms do occur, the tumor has usually spread to surrounding tissues or distant organs [4]. Most patients are inoperable at the time of diagnosis due to locally advanced disease or metastasis and experience severe abdominal pain as the disease progresses. Therefore, the treatment of patients with advanced pancreatic cancer is palliative, with the main goal of prolonging the life of patients and alleviating their pain. Many studies have shown that focused ultrasound has become a modality for the palliative treatment of pancreatic tumors. There is now a general consensus that a temperature above 55 °C maintained for more than 1 s induces nonreversible enzymatic denaturation and leads to coagulative necrosis and cell death [5,6]. The absorption of acoustic energy by biological tissues can lead to a rapid increase in the temperature of the

target area. High-intensity focused ultrasound (HIFU) aims to achieve this temperature threshold in the target area, induce coagulative necrosis, and ablate the tumor without affecting the surrounding healthy tissue.

HIFU systems usually use 'high-intensity' mode with the intensity at the focus exceeding 1000 W/cm^2 . Cavitation, boiling, and strong nonlinear acoustic emissions can be detected in this mode, which can complicate mathematical models of the focal domain and cannot accurately predict the temperature rise and the shape of coagulative necrosis [7]. In numerous studies, HIFU has been shown to be safe, effective, and practicable, but there are a few HIFU-related adverse effects [8,9]. In a study published by Strunk et al., ultrasound with a frequency of 0.8 MHz, acoustic power of 200–400 W, and a duration of more than 50 s for a single target was used to achieve palliative treatment of pancreatic cancer. Transient subcutaneous edema of the proximal upper abdominal wall was observed in nine of fifteen patients. In one patient there was superficial skin burning in the region of the navel (degree IIa) [10]. Sung et al. used focused ultrasound in the palliative treatment of pancreatic cancer with a center frequency of 0.8 MHz or 1.6 MHz and an acoustic power of 140 W–240 W; the duration of exposure depended on the monitoring of US. In forty-nine treatments, twenty-eight patients had minor complications, such as mild and severe abdominal pain with vomiting, and five patients had major complications, such as skin burn (II, III) and pancreaticoduodenal fistula [11]. During HIFU treatment, the patient's discomfort increased proportionally with increasing delivered energy [12], and pain levels seemed to be independent of the dose of anesthetic or sedation [13]. Some patients interrupted their treatment due to pain [12–14]. Even though most of the studies were performed with US-guided HIFU, standardization of energy, power, and technical parameters are lacking, and are still needed to obtain the best results at the minimum risk for the patient. Radiofrequency ablation (RFA) and irreversible electroporation (IRE) can provide palliative treatment for pancreatic cancer patients in a minimally invasive manner, but they are also limited by complications, and they should be adopted only by expert users in specialized centers of interactive pancreatology [15]. The application of moderate-intensity focused ultrasound (MIFU) in the treatment of advanced pancreatic cancer proposed in this paper is non-invasive and helps to avoid these complications.

In addition to HIFU, MIFU also plays an important role in clinical treatment. The acoustic intensity at focus induced by MIFU is below the cavitation threshold. Its intensity range is generally $100\text{--}1000 \text{ W/cm}^2$ and the peak negative pressure at the focus is 1–4 MPa [16]. Studies show that the errors caused by the complexity of cavitation and high nonlinearity can be ignored in MIFU [17,18]. During MIFU exposure, the temperature of the tissue still rises rapidly, and the general heating rate is $\leq 5 \text{ }^\circ\text{C/s}$. Damianou and Hynynen indicated that pulses lasting 10 s at an acoustic intensity of $100\text{--}400 \text{ W/cm}^2$ can be considered a threshold for tissue necrosis [19].

In this context, we studied the power setting of focused ultrasound in the palliative treatment of advanced pancreatic cancer. The primary goals of this study were to achieve accurate prediction of temperature in the target region and especially pain reduction with an improvement of the clinical condition. In this study, an infrared temperature measurement experimental system was set up to measure the temperature rise at different power in ex vivo bovine livers. This method not only has high temporal resolution and spatial resolution but also shows the temperature distribution on the two-dimensional plane and avoids the error caused by the inaccurate orientation in the axial direction when the temperature is measured by the thermocouple. The intervention of infrared glass in the experimental system made viscous heating (VH) artifacts inevitable. Viscous heating arose from the difference in density between the infrared glass and surrounding tissue; this difference in density led to relative motion (arising from the radiation force of FUS) between these two mediums and caused the viscous heating in the glass–tissue interface and then affected the measurement accuracy [20]. Therefore, based on Pennes' equation, this study established a numerical simulation model of tissue temperature rise considering the influence of VH, and verified the consistency between the simulation temperature and

the measured temperature at a power range of 4 W to 8 W (acoustic intensity range was 200 to 500 W/cm²). Considering that there is no glass in the actual treatment, a numerical simulation model was established by removing the infrared glass to predict the temperature rise of the bovine liver tissue at different power. Finally, the influence of blood perfusion on the temperature of the target area was analyzed to provide a reference for the intensity and time of the palliative treatment of tumors. It showed that the use of MIFU was conducive to effectively controlling the rise of tissue temperature until reaching the thermal damage threshold temperature (55 °C), which could more safely achieve the palliative treatment of tumors and provide a reference for the establishment of a standardized FUS dosage.

2. Materials and Methods

2.1. Ultrasound Field Calculations

The pressure distribution in the calculation domain was obtained by the nonlinear Westervelt equation [21], which is expressed as:

$$\rho \nabla \cdot \left(\frac{1}{\rho} \nabla p \right) - \frac{1}{c_0^2} \frac{\partial^2 p}{\partial t^2} + \frac{\delta}{c_0^4} \frac{\partial^3 p}{\partial t^3} + \frac{\beta}{\rho_0 c_0^4} \frac{\partial^2 p}{\partial t^2} = 0 \tag{1}$$

where ∇^2 is the Laplace operator, p is acoustic pressure, c_0 is acoustic velocity, ρ_0 is the density, β is the nonlinear coefficient, and δ is the acoustic diffusion coefficient.

The finite-difference time-domain (FDTD) method is usually used to solve the Westervelt equation, and the numerical solution of Equation (1) is calculated on the polar cylindrical grid. The ultrasonic source is modeled as a spherical shell shape about the axial symmetry of the sound source. The sound field and temperature field are calculated in axial z and radial r directions using a two-dimensional spatial grid x . The explicit FDTD method is generally used [22]. The FDTD method approximates the discrete difference of spatial and temporal partial derivatives. Each node on the computational grid is expanded from the Taylor series. The grids consist of two spatial dimensions (i, j) of uniform spacing, Δx and Δr , and a time dimension n of uniform spacing Δt . The time derivative of the Westervelt equation is calculated to the second-order accuracy:

$$\frac{\partial^2 p}{\partial t^2} \approx \frac{1}{(\Delta t)^2} \left(p_{i,j}^{n+1} - 2p_{i,j}^n + p_{i,j}^{n-1} \right) \tag{2}$$

$$\frac{\partial^3 p}{\partial t^3} \approx \frac{1}{(2\Delta t)^3} \left(6p_{i,j}^n - 23p_{i,j}^{n-1} + 34p_{i,j}^{n-2} - 24p_{i,j}^{n-3} + 8p_{i,j}^{n-4} - p_{i,j}^{n-5} \right) \tag{3}$$

The spatial difference is calculated using the fourth-order accuracy:

$$\frac{\partial p}{\partial r} \approx \frac{1}{12\Delta r} \left(-p_{i,j+2}^n + 8p_{i,j+1}^n - 8p_{i,j-1}^n + p_{i,j-2}^n \right) \tag{4}$$

$$\frac{\partial^2 p}{\partial r^2} \approx \frac{1}{12(\Delta r)^2} \left(-p_{i,j+2}^n + 16p_{i,j+1}^n - 30p_{i,j}^n + 16p_{i,j-1}^n - p_{i,j-2}^n \right) \tag{5}$$

$$\frac{\partial^2 p}{\partial x^2} \approx \frac{1}{12(\Delta x)^2} \left(-p_{i+2,j}^n + 16p_{i+1,j}^n - 30p_{i,j}^n + 16p_{i-1,j}^n - p_{i-2,j}^n \right) \tag{6}$$

The explicit difference equation of $p_{i,j}^{n+1}$ can be obtained, and finally, the acoustic field is obtained.

2.2. Temperature Profile Calculations

When focused ultrasound propagates in the tissue, part of the energy is absorbed and converted into thermal energy. At present, the most widely used heat transfer model is the

biological heat transfer model proposed by Pennes in 1948; that is, Pennes' equation [23]. Pennes' equation is usually expressed as:

$$\frac{\partial T}{\partial t} = \frac{\kappa}{\rho_0 C_t} \nabla^2 T - \frac{w_b C_b}{\rho_0 C_t} (T - T_0) + \frac{Q}{\rho_0 C_t} \tag{7}$$

where T represents the tissue temperature, ρ_0 is the density of the biological tissue, C_t is the heat capacity of the biological tissue, κ is the thermal conductivity of the biological tissue, w_b and C_b are the perfusion rate and heat capacity of blood flow, respectively, T_0 is the initial temperature of the tissue, and Q is the heat source for ultrasonic heating. Q can be expressed as:

$$Q = \frac{1}{\rho_0 c_0} \sum_{n=1}^{\infty} 2\alpha_n \langle p_n^2 \rangle \tag{8}$$

In the formula, α_n is the absorption coefficient corresponding to the n th harmonic component and $\langle \rangle$ represents the time average.

Although the infrared temperature measurement has a good spatial and temporal resolution, the viscous heating artifact caused by the infrared glass in the experimental system cannot be ignored. Viscous heating leads to a rapid increase in temperature, which affects the measurement. In this study, the effect of viscous heating artifacts is evaluated by numerical simulation based on Pennes' equation. Equation (7) is modified as follows:

$$\frac{\partial T}{\partial t} = \frac{\kappa}{\rho_0 C_t} \nabla^2 T - \frac{w_b C_b}{\rho_0 C_t} (T - T_0) + \frac{Q}{\rho_0 C_t} + \frac{Q_{vis}}{\rho_0 C_t} \tag{9}$$

The secondary heat source has modeled the viscous heating and the heat generated by the viscous force in the steady state is given by [24]:

$$Q_{vis} = \frac{U_0^2 R}{2} \frac{[1 - \{(1 + k) / [(M/M') + k]\}]^2}{1 + [k' / [(M/M') + k]]^2} \tag{10}$$

where $R = k' \omega M'$, with M' defined as the mass of tissue displaced per unit length of the glass and M is the mass per unit length of the glass. The quantities k and k' can be expressed as a function of $\phi = \frac{r_0}{2} (\frac{\omega}{\nu})^{1/2}$ with r_0 defined as the thickness of the glass and ν as the kinematic coefficient of shear viscosity $\omega = 2\pi f$, U_0 is the particle velocity at the tissue/glass interface, which can be obtained by $U_0 = p / \rho c_0$.

2.3. Simulation Model

A two-dimensional axial symmetry simulation model of the HIFU ablation was established by using the k-wave toolbox of MATLAB. The schematic diagram of the numerical simulation model without the infrared glass is shown in Figure 1. The simulation domain consists of a transducer, water, and a bovine liver. The curvature radius of the transducer was 150 mm and the aperture diameter was 95 mm. The excitation signal was a sine wave with a center frequency of 1.12 MHz. The model parameters are given in Table 1. All parameters were assumed to be constant during the focused ultrasound. The maximum size of the mesh used in the simulation was $\lambda/10$, and the mesh was further encrypted to verify the mesh's independence. After increasing the number of the mesh by 30%, the change in temperature was less than 1%. The non-linearity of the acoustic wave was calculated to order 10, and the effect of higher-order harmonics on the sound pressure distribution in the focal region was less than 0.1%.

The numerical simulation model corresponding to the infrared temperature measurement experiment is shown in Figure 2. The simulation domain includes a transducer, water, a bovine liver, and infrared glass.

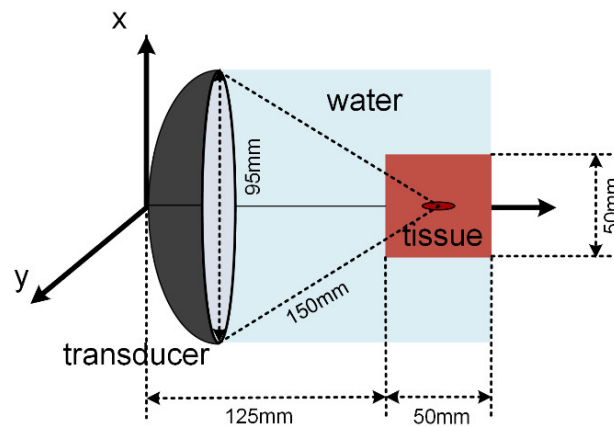


Figure 1. Schematic diagram of the simulation model without infrared glass.

Table 1. Parameters for simulation research.

Parameters		
Acoustic parameters	Frequency (MHz)	1.12
	Aperture diameter (mm)	95
	Focal length (mm)	150
Water	Sound speed (m/s)	1500
	Density (kg/m ³)	1000
	Thermal capacity (J/kg K)	4180
	Thermal conductivity (W/m K)	0.6
	Absorption coefficient (Np/m/MHz)	0.025
	Nonlinear coefficient	5
	Liver properties	Sound speed (m/s)
Density (kg/m ³)		1060
Thermal capacity (J/kg K)		3400
Thermal conductivity (W/m K)		0.45
Absorption coefficient (Np/m/MHz)		5.8
Nonlinear coefficient		6.6
Infrared glass properties		Dynamic viscosity (Pa s)
	Sound speed (m/s)	2692
	Density (kg/m ³)	1450
	Thermal capacity (J/kg K)	410
	Thermal conductivity (W/m K)	11.72
	Absorption coefficient (Np/m/MHz)	0
Geometrical specifications	Liver diameter (mm)	50
	Liver length (mm)	25

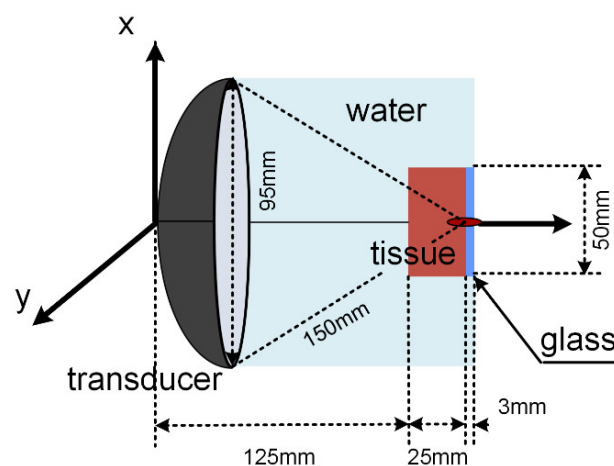


Figure 2. Schematic diagram of the simulation model with infrared glass.

2.4. Experimental Setup

A fresh bovine liver was collected from a local slaughterhouse and the whole experiment was conducted within 8 h after the cattle was slaughtered. The liver tissue was cut into a cylindrical shape with a diameter of 50 mm and a thickness of 25 mm. The cylinders were placed in a pressure chamber with degassing water and the pressure chamber was sealed. The tissue was degassed for 40 min with a pump with a vacuum degree of -0.9 .

The experimental system is shown in Figure 3. The excitation signal was generated by the arbitrary signal generator (DG5072, RIGOL, Beijing, China). The signal passed through the power amplifier (AR800 W, Amplifier Research, Souderton, PA, USA) and drove the transducer to irradiate the continuous wave (the transducer parameters were consistent with those in the simulation). The transducer and tissue were immersed in degassed water, and the upper surface of a bovine liver tissue sample was attached to the infrared glass and placed in focus. The infrared glass was placed in the field of view of a 50 Hz infrared camera (K23a17, HJKIR, Wuhan, China) and the temperature distribution of the bovine liver at different power-focused ultrasounds was recorded.

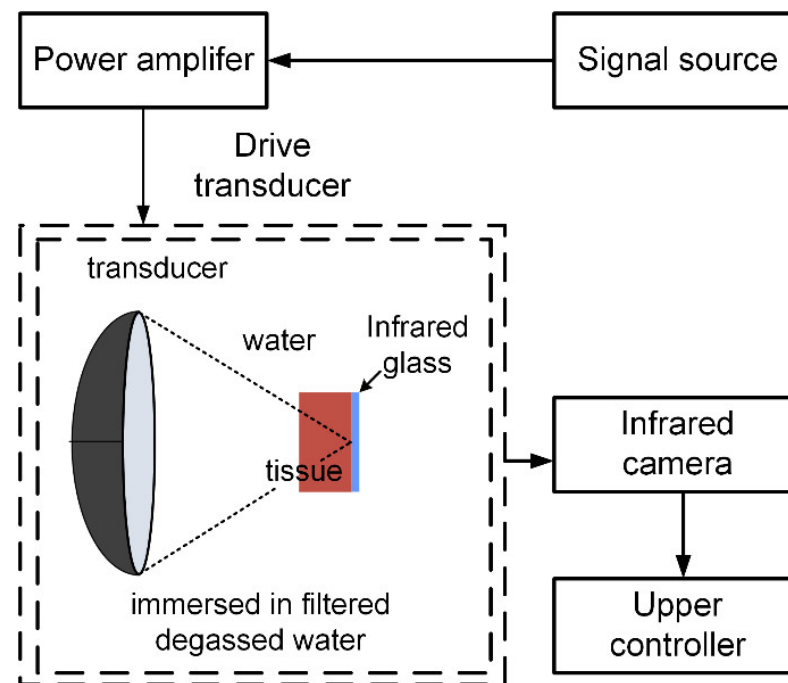


Figure 3. Schematic diagram of the experimental system.

3. Results and Discussion

The initial temperature of the experiment and simulation was $30\text{ }^{\circ}\text{C}$. Figure 4 shows the measured temperature rise of the bovine liver exposed for 5 s at 10 W, 40 W, and 125 W acoustic power. The maximum acoustic intensity at the focus was 500, 3000, and $10,000\text{ W}/\text{cm}^2$, respectively.

Under three kinds of power, the temperature of the bovine liver increased rapidly at the initial stage, which was caused by the cavitation effect and viscous heating of the tissue and glass at 125 W and 40 W. When the power was 10 W (lower than the cavitation threshold), this was due to viscous heating. When the power was 125 W, the temperature elevation of the tissue was rapidly above $60\text{ }^{\circ}\text{C}$, which indicated that cavitation occurred at the beginning of sonication. Due to thermal equilibrium, the temperature of the tissue reached its maximum and then decreased slightly until the end of the sonication. This trend was similar to that reported by Jensen et al. [25]. The temperature increase rate of the bovine liver at 40 W was slower than that at 125 W and reached the maximum temperature of $77\text{ }^{\circ}\text{C}$ within 1 s; then, the temperature remained almost unchanged. This trend was similar to that reported by Chang et al. [26]. When the power was 10 W (below the threshold of

acoustic cavitation), the temperature of the tissue increased rapidly at first and then slowly under the effect of viscous heating, and the temperature increased steadily to 43 °C within 5 s. It can be seen that when the intensity of focused ultrasound exceeded the cavitation threshold, the time of heating to the maximum temperature decreased with the increased power. It was difficult to predict the temperature of the tissue during sonication, which was closely related to some complex factors such as cavitation bubbles, thermal necrosis, etc. These processes such as cavitation, boiling, and their effects on temperature have not been accurately evaluated, and are not included in the classical numerical simulation model of the HIFU. Therefore, if the intensity above the cavitation threshold was applied to the tissue, for example, 125 W, its temperature prediction after several milliseconds might not be reliable. The mean temperature increase rate of the tissue was more than 30 °C/s in the first 1 s of the sonication at 40 W, and the temperature was difficult to control accurately. When the intensity of focused ultrasound was lower than the cavitation threshold (the power was 10 W and the intensity was within the MIFU range), the temperature increased steadily. At this power, the main factors that make the temperature increase were the thermal effect and viscous heating, which facilitated the prediction and control of the temperature. The relationship between temperature and exposure time of the bovine liver at different power (within the MIFU range) was studied as follows.

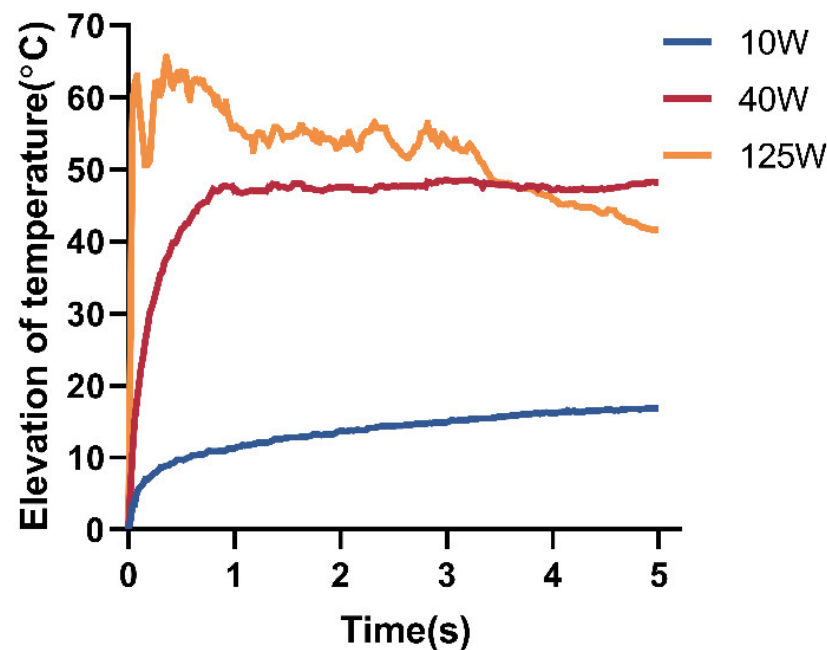


Figure 4. The measured temperature rise of the bovine liver tissue was exposed continuously for 5 s at 10 W, 40 W, and 125 W.

Figure 5 shows the measured, simulated, and modified predicted temperature elevation curves of the bovine liver with time during 40 s of sonication at 4 W, 6 W, and 8 W (200–500 W/cm², MIFU). First, the temperature measured was compared with the temperature calculated by numerical simulation considering VH to verify the correctness of the secondary heat source Q_{vis} . The maximum relative error was 4.1%. The measured temperature elevation after sonication was 12.9 °C (power = 4 W), 18.4 °C (power = 6 W), and 30.8 °C (power = 8 W). The simulated temperature elevation after sonication was 13.6 °C (power = 4 W), 19.4 °C (power = 6 W), and 28.3 °C (power = 8 W). With the increase in power, viscous heating would make the tissue rise to a higher temperature within 5 s. After a certain period of time, the contribution of viscous heating to temperature reached the plateau, and further temperature rise was mainly caused by absorbing acoustic energy.

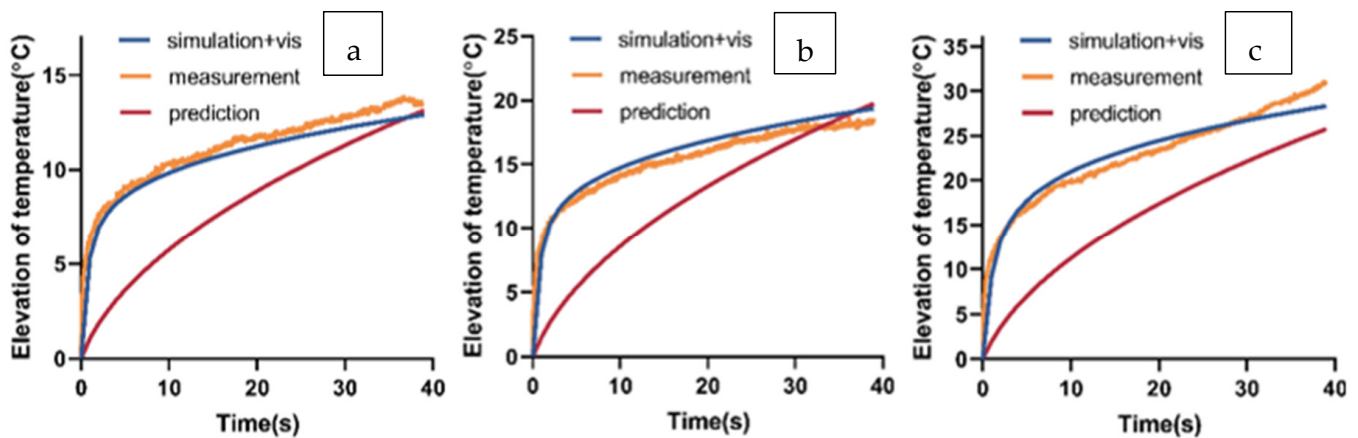


Figure 5. Temperature elevations at focus (a) 4 W, (b) 6 W, and (c) 8 W. The yellow solid lines present the measured temperature (measurement). The blue solid lines present the simulated temperature considering viscous heating (simulation + vis). The red solid lines present the predicted temperature (without glass and without VH) in the pure bovine liver (prediction).

Furthermore, viscous heating was removed from the numerical simulation model, and the temperature elevation of the bovine liver is given in Figure 5. The temperature rise curves were approximately linear (without the infrared glass). The difference between the predicted temperature and the measured temperature reached the maximum within 5 s, and then gradually decreased. The modified predicted temperature elevation after sonication was 13.1 °C (power = 4 W), 19.8 °C (power = 6 W), and 25.4 °C (power = 8 W).

The width of the acoustic focal area (-3 dB acoustic field) of the transducer used in this study is 2.95 mm. Figure 6 shows the temperature elevation at 1.5 mm away from the focus in the direction of the focal plane. It can be seen in Figure 6 that the simulated results considering viscous heating were close to the measured results, and the maximum relative error was 6.7%. After removing the viscous heating from the numerical simulation model, the predicted temperature of the bovine liver at 4 W, 6 W, and 8 W reached 40 °C, 45.8 °C, and 49 °C, respectively, at the end of sonication, which was 3~4 °C lower than the temperature at focus.

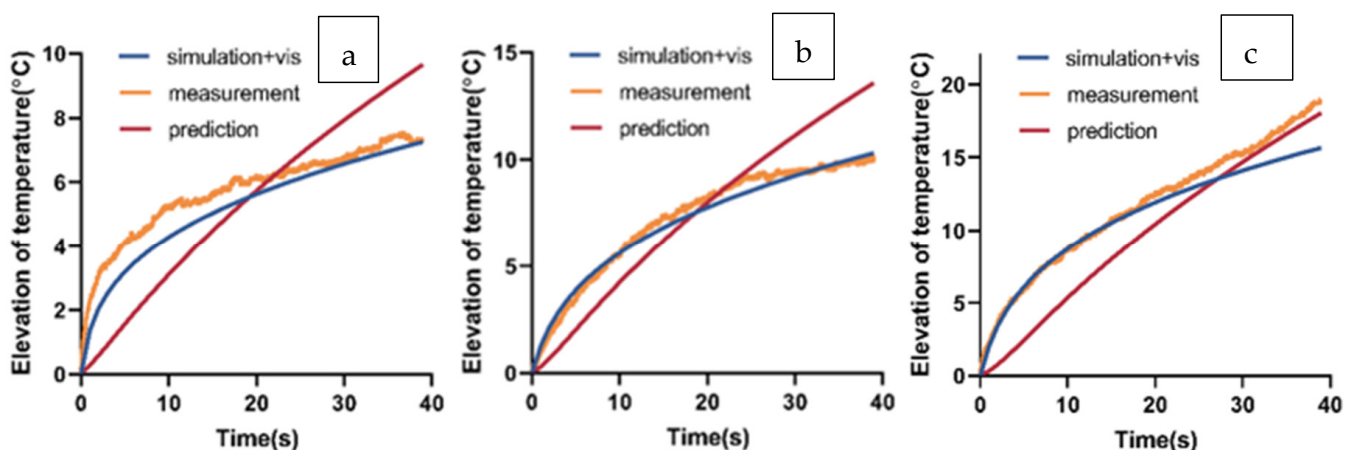


Figure 6. Temperature elevations at 1.5 mm away from the focus (a) 4 W, (b) 6 W, and (c) 8 W. The yellow solid lines present the measured temperature (measurement). The blue solid lines present the simulated temperature considering viscous heating (simulation + vis). The red solid lines present the predicted temperature (without glass and without VH) in the pure bovine liver (prediction).

These studies were based on an ex vivo bovine liver without considering blood perfusion. However, blood can take away part of the heat and reduce the efficacy of FUS.

This study further quantified the effect of blood perfusion on the efficacy of FUS. The temperature at focus after sonication (40 s) and the temperature at 1.5 mm from the focus (Figure 7) at different power were calculated by numerical simulation, whether or not blood perfusion was considered in both cases. As shown by the best-fitting line, the relationship between temperature and power was approximately linear in the MIFU range.

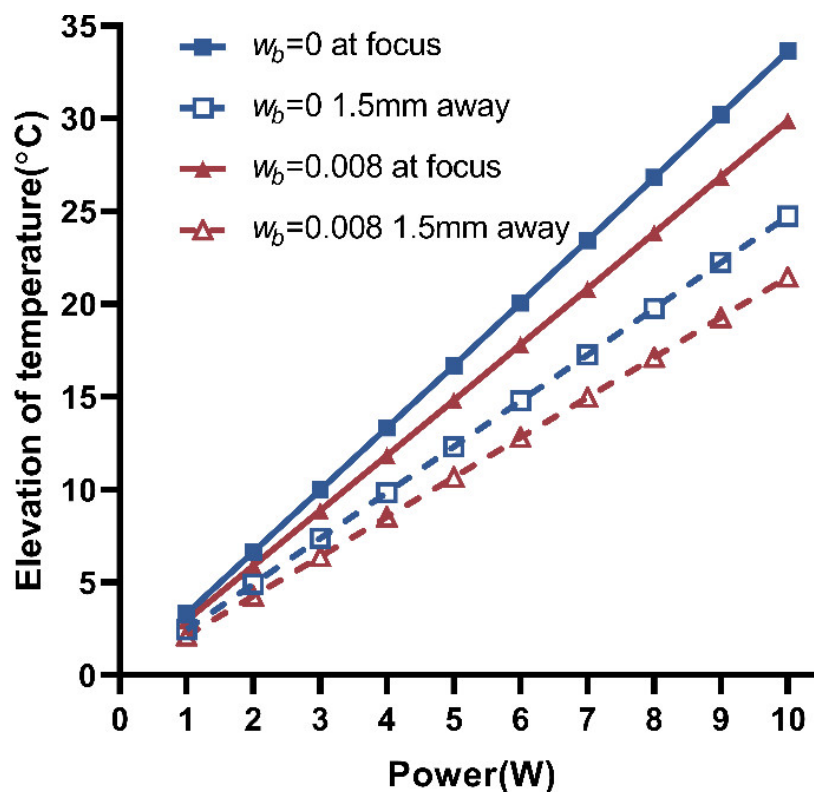


Figure 7. The temperature (predicted) of the bovine liver at 40 s at different power. The blue solid line presents the temperature at focus when ignoring blood perfusion ($w_b = 0$, at focus), the blue dotted line presents the temperature at 1.5 mm away from the focus when ignoring blood perfusion ($w_b = 0$, 1.5 mm away), the red solid line presents the temperature at focus when considering blood perfusion ($w_b = 0.008$, at focus), and the red dotted line presents the temperature at 1.5 mm away from the focus when considering blood perfusion ($w_b = 0.008$, 1.5 mm away). When the blood perfusion was ignored, for a 1 W increase in power, the temperature at focus increased by 3.3 °C after sonication, and the temperature at 1.5 mm away from the focus increased by 2.5 °C. When the blood perfusion was considered ($w_b = 0.008$), the temperature at focus increased by 3 °C after sonication, and the temperature at 1.5 mm away from the focus increased by 2.1 °C. With the increase in power, the temperature difference between the focus and at 1.5 mm from the focus gradually increased, and the effect of blood perfusion on the temperature gradually increased.

4. Conclusions

The infrared temperature measurement system was set up to measure the temperature elevation of a bovine liver at different power. The temperature rise curves at the focus fall into three broad categories. 1. At a power of 125 W ($I \approx 10,000$ W/cm²), the tissue temperature at focus rose rapidly to the maximum temperature (>90 °C) within tens of milliseconds and then fluctuated slightly. 2. When the power was reduced to 40 W ($I \approx 3000$ W/cm²), the temperature rose rapidly in a short time, reached the maximum temperature of about 77 °C within 1 s, and was almost kept unchanged. The temperature rise rate of the tissue was still more than 30 °C/s. 3. When the power was in the range of 4 W to 8 W (MIFU, $240 \leq I \leq 500$ W/cm²), the temperature increased steadily. At the end of sonication, the measured temperature was controlled below 60 °C.

Accurate prediction before operation and optimal control during treatment are the keys to achieving therapeutic effects and avoiding adverse effects when focused ultrasound is applied in tumor ablation. The development of acoustic cavitation, boiling, and shielding of large bubbles and their effects on temperature has not been accurately evaluated and is not included in the classical numerical simulation model. Therefore, it might not be reliable to predict the temperature when the intensity of 1000 W/cm^2 was applied to the tissue; high temperature would lead to tissue boiling and bubble formation and might induce more undefined and less predictable necrosis. These would challenge the effective temperature control during the treatment [27]. For focused ultrasound (MIFU) with an intensity below 1000 W/cm^2 , the intensity range was below the cavitation threshold and the temperature increase mainly depended on the thermal effect, and it was easy to assess and predict temperature during treatment. The goal of this study was to control tissue temperature rise until reaching the threshold for thermal necrosis ($55 \text{ }^\circ\text{C}$), which could more safely achieve the palliative treatment of tumors. Therefore, this study focused on the intensity range of moderate-intensity focused ultrasound ($100 \text{ W/cm}^2 \leq I \leq 1000 \text{ W/cm}^2$), and discussed the temperature rise at different power in a bovine liver. The simulated and measured results showed that (1) the temperature of the tissue induced by the MIFU at the end of sonication was linearly related to the power and (2) the effect of blood perfusion on temperature increased with the power increase.

Fabiano et al. described that focused ultrasound could reach and keep the required temperature at low acoustic power, which might reduce potential adverse effects and patients' discomfort [28]. This paper further quantified the appropriate intensity range for tumor ablation of advanced pancreatic cancer. The MIFU is easier to control the temperature than the HIFU while ensuring treatment efficiency, which is conducive to accurate prediction, and is safer and more suitable for the palliative treatment of tumors.

This study is based on homogenous bovine liver tissues. In clinical treatment, the situation of each patient is different, and the setting of treatment parameters varies from person to person. In future research, the parameters used in clinical treatment cases can be considered for the temperature simulation to evaluate the impact of different sound channels on the treatment effect.

Author Contributions: Conceptualization, S.T. and Y.W.; Methodology, J.T.; Software, P.Z.; Validation, X.G. and Y.Y.; Writing—Original Draft Preparation, S.T.; Supervision, Y.W. All authors have read and agreed to the published version of the manuscript.

Funding: This research received no external funding.

Institutional Review Board Statement: Not applicable.

Informed Consent Statement: Not applicable.

Data Availability Statement: Not applicable.

Acknowledgments: The authors gratefully acknowledge the support of the Science and Technology Plan Projects Department of Education of Zhejiang Province (Y202147977).

Conflicts of Interest: The authors declare no conflict of interest.

References

1. Rahib, L.; Smith, B.D.; Aizenberg, R.; Rosenzweig, A.B.; Fleshman, J.M.; Matrisian, L.M. Projecting cancer incidence and deaths to 2030: The unexpected burden of thyroid, liver, and pancreas cancers in the United States. *Cancer Res.* **2014**, *74*, 2913–2921. [[CrossRef](#)] [[PubMed](#)]
2. Siegel, R.L.; Miller, K.D.; Fuchs, H.E.; Jemal, A. Cancer statistics, 2022. *CA Cancer J. Clin.* **2022**, *72*, 7–33. [[CrossRef](#)]
3. Ullman, N.A.; Burchard, P.R.; Dunne, R.F.; Linehan, D.C. Immunologic strategies in pancreatic cancer: Making cold tumors hot. *J. Clin. Oncol.* **2022**, *40*, 2789. [[CrossRef](#)] [[PubMed](#)]
4. Khokhlova, T.D.; Hwang, J.H. HIFU for palliative treatment of pancreatic cancer. In *Therapeutic Ultrasound*; Springer: Cham, Switzerland, 2016; pp. 83–95.
5. Ter Haar, G.; Coussios, C. High intensity focused ultrasound: Physical principles and devices. *Int. J. Hyperther.* **2007**, *23*, 89–104. [[CrossRef](#)] [[PubMed](#)]

6. Pacella, C.M.; Bizzarri, G.; Guglielmi, R.; Anelli, V.; Bianchini, A.; Crescenzi, A.; Pacella, S.; Papini, E. Thyroid tissue: US-guided percutaneous interstitial laser ablation—A feasibility study. *Radiology* **2000**, *217*, 673–677. [[CrossRef](#)]
7. Khokhlova, V.A.; Bailey, M.R.; Reed, J.A.; Cunitz, B.W.; Kaczkowski, P.J.; Crum, L.A. Effects of nonlinear propagation, cavitation, and boiling in lesion formation by high intensity focused ultrasound in a gel phantom. *J. Acoust. Soc. Am.* **2006**, *19*, 1834–1848. [[CrossRef](#)]
8. Lv, W.; Yan, T.; Wang, G.; Zhao, W.; Zhang, T.; Zhou, D. High-intensity focused ultrasound therapy in combination with gemcitabine for unresectable pancreatic carcinoma. *Ther. Clin. Risk Manag.* **2016**, *12*, 687.
9. Dababou, S.; Marrocchio, C.; Rosenberg, J.; Bitton, R.; Pauly, K.B.; Napoli, A.; Hwang, J.H.; Ghanouni, P. A meta-analysis of palliative treatment of pancreatic cancer with high intensity focused ultrasound. *J. Ther. Ultras.* **2017**, *5*, 9. [[CrossRef](#)]
10. Strunk, H.M.; Henseler, J.; Rauch, M.; Mucke, M.; Kukuk, G.; Cuhls, H.; Radbruch, L.; Zhang, L.; Schild, H.H.; Marinova, M. Clinical use of high-intensity focused ultrasound (HIFU) for tumor and pain reduction in advanced pancreatic cancer. In *RöFo-Fortschritte auf dem Gebiet der Röntgenstrahlen und der bildgebenden Verfahren*; Georg Thieme Verlag KG: Stuttgart, Germany, 2016; Volume 188, pp. 662–670.
11. Sung, H.Y.; Jung, S.E.; Cho, S.H.; Zhou, K.; Han, J.Y.; Han, S.T.; Kim, J.I.; Kim, J.K.; Choi, J.Y.; Yoon, S.K.; et al. Long-term outcome of high-intensity focused ultrasound in advanced pancreatic cancer. *Pancreas* **2011**, *40*, 1080–1086. [[CrossRef](#)]
12. Esnault, O.; Franc, B.; Ménégau, F.; Rouxel, A.; Kerviler, E.D.; Bourrier, P.; Lacoste, F.; Chapelon, J.Y.; Leenhardt, L. High-intensity focused ultrasound ablation of thyroid nodules: First human feasibility study. *Thyroid* **2011**, *21*, 965–973. [[CrossRef](#)] [[PubMed](#)]
13. Korkusuz, H.; Fehre, N.; Sennert, M.; Happel, C.; Grunwald, F. Early assessment of high-intensity focused ultrasound treatment of benign thyroid nodules by scintigraphic means. *J. Ther. Ultras.* **2014**, *2*, 18. [[CrossRef](#)] [[PubMed](#)]
14. Lang, B.H.H.; Woo, Y.C.; Chiu, K.W.H. Single-session high-intensity focused ultrasound treatment in large-sized benign thyroid nodules. *Thyroid* **2017**, *27*, 714–721. [[CrossRef](#)] [[PubMed](#)]
15. Paiella, S.; De Pastena, M.; D’Onofrio, M.; Crinò, S.F.; Pan, T.L.; De Robertis, R.; Elio, G.; Martone, E.; Salvia, R. Palliative therapy in pancreatic cancer—Interventional treatment with radiofrequency ablation/irreversible electroporation. *Transl. Gastroenterol. Hepatol.* **2018**, *3*, 80. [[CrossRef](#)]
16. Hariharan, P.; Myers, M.R.; Banerjee, R.K. HIFU procedures at moderate intensities—Effect of large blood vessels. *Phys. Med. Biol.* **2007**, *52*, 3493. [[CrossRef](#)]
17. Xu, Z.; Fowlkes, J.B.; Ludomirsky, A.; Cain, C.A. Investigation of intensity thresholds for ultrasound tissue erosion. *Ultrasound Med. Biol.* **2005**, *31*, 1673–1682. [[CrossRef](#)]
18. Mahoney, K.; Fjield, T.; McDannold, N.; Clement, G.; Hynynen, K. Comparison of modelled and observed in vivo temperature elevations induced by focused ultrasound: Implications for treatment planning. *Phys. Med. Biol.* **2001**, *46*, 1785. [[CrossRef](#)]
19. Damianou, C.; Hynynen, K. The effect of various physical parameters on the size and shape of necrosed tissue volume during ultrasound surgery. *J. Acoust. Soc. Am.* **1994**, *95*, 1641–1649. [[CrossRef](#)]
20. Karaböce, B.; Çetin, E.; Durmuş, H.O.; Özdingiş, M.; Korkmaz, H.; Altun, J.; Argun, S. Experimental investigations of viscous heating effect of thermocouples under focused ultrasound applications. In Proceedings of the 2017 IEEE International Symposium on Medical Measurements and Applications (MeMeA), Rochester, MN, USA, 7–10 May 2017; pp. 88–93.
21. Norton, G.V.; Purrington, R.D. The Westervelt equation with viscous attenuation versus a causal propagation operator: A numerical comparison. *J. Sound. Vib.* **2009**, *327*, 163–172. [[CrossRef](#)]
22. Yee, K. Numerical solution of initial boundary value problems involving Maxwell’s equations in isotropic media. *IEEE Trans. Antennas Propag.* **1966**, *14*, 302–307.
23. Pennes, H.H. Analysis of tissue and arterial blood temperatures in the resting human forearm. *J. Appl. Physiol.* **1948**, *1*, 93–122. [[CrossRef](#)] [[PubMed](#)]
24. Tiennot, T.; Kamimura, H.A.S.; Lee, S.A.; Aurup, C.; Konofagou, E.E. Numerical modeling of ultrasound heating for the correction of viscous heating artifacts in soft tissue temperature measurements. *Appl. Phys. Lett.* **2019**, *114*, 203702. [[CrossRef](#)] [[PubMed](#)]
25. Jensen, C.R.; Cleveland, R.O.; Coussios, C.C. Real-time temperature estimation and monitoring of HIFU ablation through a combined modeling and passive acoustic mapping approach. *Phys. Med. Biol.* **2013**, *58*, 5833. [[CrossRef](#)] [[PubMed](#)]
26. Chang, N.; Lu, S.; Qin, D.; Xu, T.; Han, M.; Wang, S.; Wan, M. Efficient and controllable thermal ablation induced by short-pulsed HIFU sequence assisted with perfluorohexane nanodroplets. *Ultrason Sonochem.* **2018**, *45*, 57–64. [[CrossRef](#)]
27. Chen, L.; ter Haar, G.; Hill, C.R. Influence of ablated tissue on the formation of high-intensity focused ultrasound lesions. *Ultrasound Med. Biol.* **1997**, *23*, 921–931. [[CrossRef](#)]
28. Bini, F.; Trimboli, P.; Marinozzi, F.; Giovanella, L. Treatment of benign thyroid nodules by high intensity focused ultrasound (HIFU) at different acoustic powers: A study on in-silico phantom. *Endocrine* **2018**, *59*, 506–509. [[CrossRef](#)]

Disclaimer/Publisher’s Note: The statements, opinions and data contained in all publications are solely those of the individual author(s) and contributor(s) and not of MDPI and/or the editor(s). MDPI and/or the editor(s) disclaim responsibility for any injury to people or property resulting from any ideas, methods, instructions or products referred to in the content.